Compressible 3D-simulations of spherical bubble collapses in viscoelastic fluids

Christian Lang [1]*, Steffen J. Schmidt [1] and Nikolaus A. Adams [1]

[1] Chair of Aerodynamics and Fluid Mechanics, Technical University of Munich, Germany

Abstract: We present fully compressible simulations of spherical vapor bubble collapses in viscoelastic fluids. A density based finite volume solver with explicit time integration and different viscoelastic constitutive models is employed to show the influence of elasticity and the distinct collapse behavior obtained with different viscoelastic models.

Keywords: Viscoelasticity, non-Newtonian, cavitation, single-fluid model, spherical bubble collapse, compressible flow, finite volumes

1. Introduction

Already in 1970 [1] revealed that viscoelasticity can have crucial influence on the bubble collapse and ascertained that it can be retarded and oscillatory motion initiated by the viscoelastic contribution of the Maxwell fluid surrounding a void. Especially in biomedical processes such as histotripsy and lithotripsy, where bubble dynamics often occur in viscoelastic media, one has to include its influence. Several studies revealed an noticeable effect of viscoelasticity on the bubble collapse behavior[2]–[6]. Furthermore [7], [8] examined bubble dynamics in viscoelastic media and found out that compressibility affects the dynamics as well. All of the aforementioned studies are conducted on the basis of 1D formulations of the governing equations and the assumption of incompressibility at least of the liquid in the vicinity of the bubble (see [7], [8]) by describing the dynamics with a formulation similar to the Rayleigh-Plesset or Keller-Miksis equation [9], [10]. Comparisons of our fully compressible 3D simulations show significant deviations from those obtained with such 1D approaches what led us to conduct various simulations of the spherical bubble collapse for different viscoelastic models and material parameters.

2. Model and numerical method

We apply the conservation equations for 3D compressible barotropic flow, namely the mass and momentum conservation equation together with an Oldroyd-like viscoelastic constitutive model. The governing differential equations read

$$\begin{aligned} \frac{\partial \rho}{\partial t} + \operatorname{div}(\rho \mathbf{u}) &= 0 \\ \frac{\partial (\rho \mathbf{u})}{\partial t} + \operatorname{div}(\rho \mathbf{u} \otimes \mathbf{u}) &= \operatorname{div}\left(-p\mathbf{I} + 2\mu_S \mathbf{D}^d + \boldsymbol{\tau}_M\right) \\ \boldsymbol{\tau}_M + \lambda \check{\boldsymbol{\tau}}_M + f\left(\boldsymbol{\tau}_M, \mathbf{D}^d\right)\boldsymbol{\tau}_M &= 2\mu_M \mathbf{D}^d, \end{aligned} \tag{1}$$

where ρ, p and $\mathbf{u}$ represent the density, the pressure and the velocity, respectively. $\mathbf{D}^d$ is the deviatoric part of the strain rate tensor. μ_S describes the solvent viscosity. The viscosity of the polymeric liquid μ_M is denoted as Maxwell viscosity and is responsible for the viscoelastic contribution. $\boldsymbol{\tau}_M$ represents the stress tensor of the Maxwell part of the constitutive model. Via the additional term $f(\boldsymbol{\tau}_M, \mathbf{D}^d)$, the simplified linear Phan-Thien Tanner model (LPTT) [11] and the simplified exponential Phan-Thien Tanner model (EPTT) [12] are implemented. Both originate from the network theory and incorporate shear-thinning effects and a bounded extensional viscosity. For the LPTT the additional term reads $f = \epsilon\lambda tr(\boldsymbol{\tau}_M)/\mu_M$

* Corresponding Author: Christian Lang, c.lang@tum.de

and for the EPTT it is defined as $f = \exp(\epsilon\lambda tr(\boldsymbol{\tau}_M)/\mu_M) - 1$, where ϵ represents the extensibility parameter. If the additional term f is neglected the Oldroyd-B (OLD-B) model [13] is regained. Furthermore, when we omit the solvent viscosity ($\mu_S = 0$), we retrieve the upper convected Maxwell model (UCM). $\check{\boldsymbol{\tau}}_M$ represents an objective time derivative of the additional Maxwell stress. The appropriate objective rate in the context of compressible flow is the Truesdell rate

$$\check{\boldsymbol{\tau}}_M = \frac{D\boldsymbol{\tau}_M}{Dt} - \nabla\mathbf{u}\cdot\boldsymbol{\tau}_M - \boldsymbol{\tau}_M\cdot\nabla\mathbf{u}^T + (\nabla\cdot\mathbf{u})\boldsymbol{\tau}_M. \tag{2}$$

All mentioned quantities within the conservative equations can be understood as volume averaged homogenous water-vapor mixture quantities since we make use of a single-fluid where both phases are in mechanical and thermodynamic equilibrium and do not exhibit time delay in evaporation and condensation. The mixture density is composed of vapor and liquid density as follows

$$\rho = \alpha\rho_v + (1-\alpha)\alpha_l. \tag{3}$$

The pressure is calculated dependent on the current phase composition. For pure liquid a modified Tait equation is employed. If two phases are present, we exploit the barotropic definition of speed of sound to obtain the pressure by integration as performed in [14].

The spatial discretization follows a finite volume framework where the convective and diffusive (viscous) fluxes at the cell faces are treated separately. For the convective fluxes an upwind-biased approximate Riemann solver is applied [15], [16]. The diffusive fluxes are calculated by a central-difference scheme. Explicit time integration is performed by a four step Runge-Kutta method as explained in [17] in order to resolve compressible wave dynamics and corresponding effects. The time step calculation is adapted due to the wave speeds modified by viscoelasticity.

3. Results

We exploit the spherical symmetry and conduct our simulations on one eighth of the bubble. The bubble is discretized with a resolution of 50 cells per radius. We define the following dimensionless numbers to describe viscoelastic bubble collapse

$$Re = \frac{R_0\sqrt{\rho\Delta p}}{\mu_0}, \qquad De = \frac{\lambda}{R_0}\sqrt{\frac{\Delta p}{\rho}}, \qquad \beta = \frac{\mu_S}{\mu_0}, \tag{4}$$

where the Reynolds number Re is calculated with the combined viscosity of solvent (Newtonian) and Maxwell viscosity $\mu_0 = \mu_S + \mu_M$. The Deborah number De characterizes the elastic influence, i.e. high Deborah numbers are related with a long relaxation time and a strong elastic contribution. β puts the solvent in relation to the total viscosity. For all the simulations with solvent viscosity, a value of $\beta = 0.1$ is used like commonly done in existing studies. By using the UCM model, solvent viscosity is not existent and β is obsolete.

Firstly, we show the evolution of the bubble size for the UCM viscoelastic model and Newtonian fluid with $Re = De = 1$. In Fig. 1 the nondimensionalized radius $r^* = r/R_0$ of the bubble is plotted against dimensionless time $t^* = t/T_0$ with $T_0 = R_0\sqrt{\rho/\Delta p}$. For the UCM model it is possible to solve the 1D Rayleigh-Plesset and the Keller-Miksis equation with the help of an ODE-based solver, too. Thus, we show the results of 1D simulations performed with the ODE solver and the 3D results of our solver for this particular case. The evolution of the bubble size shows clear differences when comparing the Newtonian

and the viscoelastic case. Besides, it is observable that the results of the 3D simulations clearly deviate from those obtained with the 1D approach. The differences could possibly be traced back to the neglection of compressible effects within the 1D equations. By using the Rayleigh-Plesset equation compressible effects are completely neglected whereas in the Keller-Miksis equation, compressibility is considered in the far-field of the bubble and the near-field is treated as incompressible.

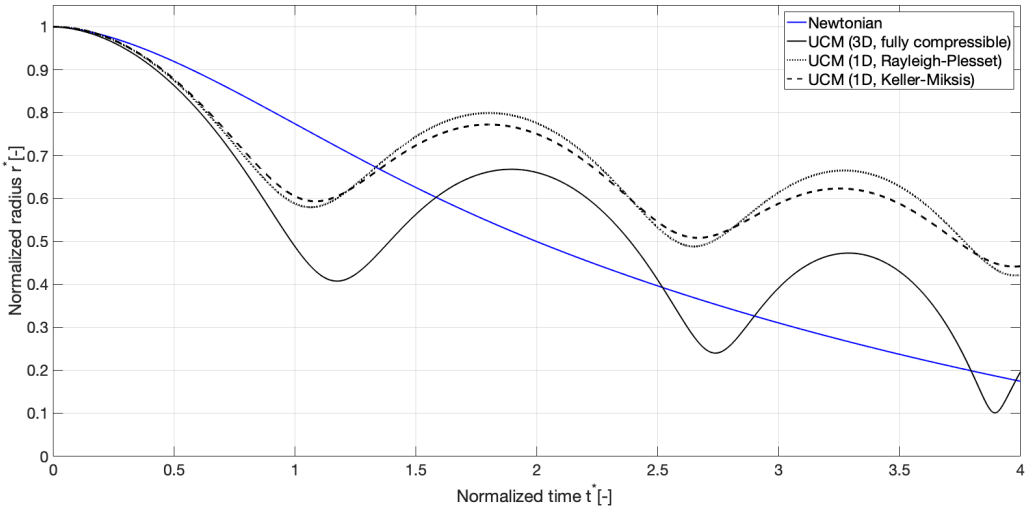

Figure 1. Influence of viscoelasticity on the bubble collapse. Evolution of nondimensional bubble radius for Newtonian (Re = 1) against UCM viscoelastic fluid (Re = 1, De = 1). Fully compressible 3D simulations are compared with results obtained by 1D simulations obtained with the Rayleigh-Plesset and the Keller-Miksis formulation, respectively.

Subsequently, we examine the influence of viscoelasticity on the bubble collapse for the UCM and the OLD-B fluid. In Fig. 2 the evolution of the bubble size is presented for different Deborah numbers, i.e. for different elasticities. As already stated in [6], we can also observe that a rebound is only occurring for a narrow band of the product of ReDe. Hence, we exclusively show the results for ReDe∼1, too.

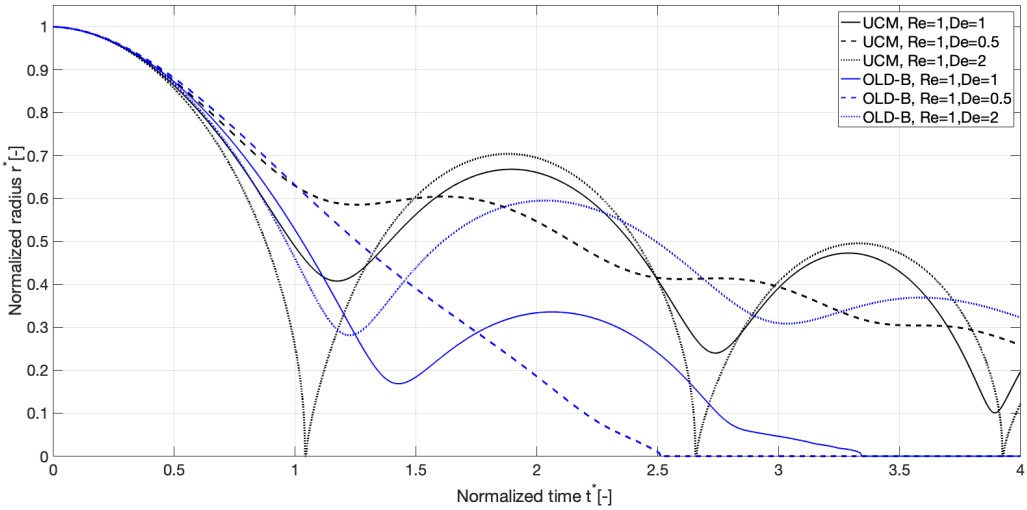

Figure 2. The influence of elasticity (relaxation time) on the bubble collapse. Evolution of the bubble radius for UCM (black) and OLD-B (blue) model at fixed Re = 1 for three different Deborah numbers.

We can ascertain that increasing the elasticity (De ↑) leads to an acceleration of the first collapse. This is reasonable since the buildup of the polymeric stress is retarded and therefore less viscous dissipation takes place. At the same time, an increased relaxation time leads to larger maximum values of the radius after the first rebound since less energy is dissipated and the fluid is able to store more elastic energy. Besides that, the OLD-B fluid exhibits a slower collapse in the initial stages. This can be traced back to the nature of the model where a viscous force is already initially present in contrast to the UCM fluid. For all parameters the collapse of the OLD-B fluid shows smaller rebound radii for the rebounds. For a small relaxation time (De = 0.5) there is even no rebound observable at all for OLD-B while the UCM still exposes rebounds and a much slower compression of the vapor bubble. For the UCM fluid we examine the influence of elasticity on the intensity of the collapse in more detail in terms of the magnitude of velocity right after the first rebound ($t = 4 \cdot 10^{-6}$ s) in Fig. 3. We can clearly see that the velocities during the first rebound are much higher with increasing elasticity.

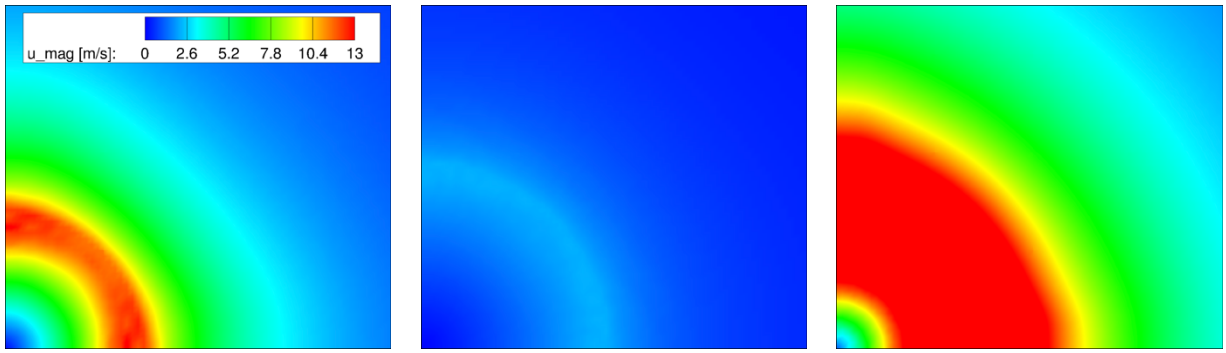

Figure 3. Contour of the magnitude of velocity $\|\mathbf{u}\|$ right after the first collapse ($t = 4 \cdot 10^{-6}$ s) for three different elasticities at Re = 1 (slices through the center of the bubble). (a) De = 1, (b) De = 0.5, (c) De = 2.

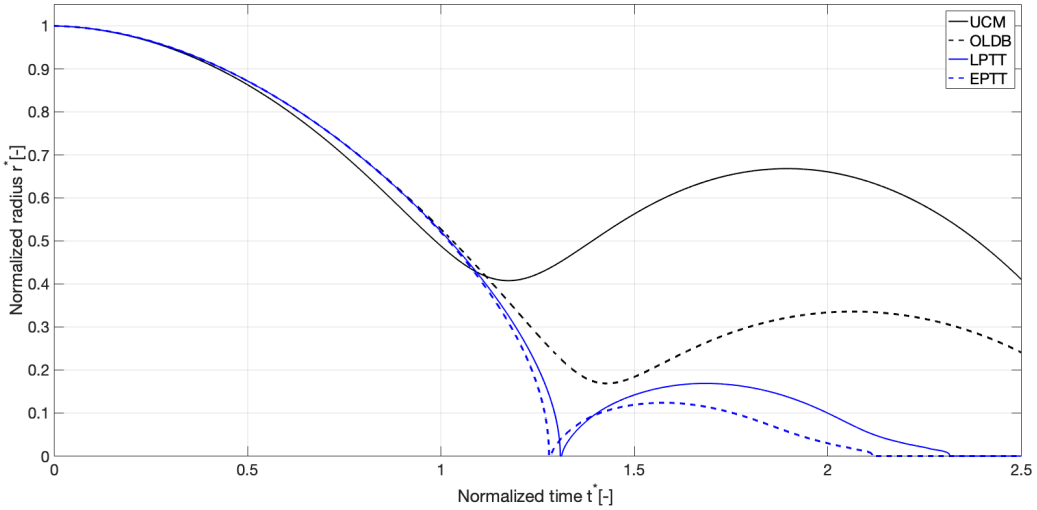

Figure 4. Bubble collapse behavior for the different implemented viscoelastic models at Re = 1, De = 1.

Finally, a comparison of the collapse behavior for the different implemented viscoelastic models at $\mathrm{Re} = 1,\ \mathrm{De} = 1$ is shown in Fig. 4. The behavior of the LPTT/EPTT models is of particular interest since these models predict shear-thinning of the viscosity and the first normal stress difference. Both models are based on the network theory. The reason for the shear-thinning property is the destruction of junctions within the polymer network. For the PTT models, an extensibility parameter of $\epsilon = 0.25$ was chosen. The shear-thinning behavior involves decreased damping, especially at the later stages of the collapse, since the viscosity is decreased with increasing shear rate. Due to the decreased viscosity the collapse mimics the behavior of an inertia dominated Rayleigh collapse at the end of the first collapse. The shear-thinning is even more emphasized in the case of the EPTT since an exponential term is used to modify the Maxwell stress transport equation.

References

[1] H. S. Fogler and J. D. Goddard, "Collapse of spherical cavities in viscoelastic fluids," *Phys. Fluids*, vol. 13, no. 5, pp. 1135–1141, 1970.
[2] C. Kim, "Collapse of Spherical Bubbles in Maxwell fluids," *J. Nonnewton. Fluid Mech.*, vol. 55, 1994.
[3] E. A. Brujan, "A first-order model for bubble dynamics in a compressible viscoelastic liquid," *J. Nonnewton. Fluid Mech.*, vol. 84, no. 1, pp. 83–103, 1999.
[4] J. S. Allen and R. A. Roy, "Dynamics of gas bubbles in viscoelastic fluids. II. Nonlinear viscoelasticity," *J. Acoust. Soc. Am.*, vol. 107, no. 6, pp. 3167–3178, 2000.
[5] J. S. Allen and R. A. Roy, "Dynamics of gas bubbles in viscoelastic fluids. I. Linear viscoelasticity," *J. Acoust. Soc. Am.*, vol. 107, no. 6, pp. 3167–3178, 2000.
[6] S. J. Lind and T. N. Phillips, "Spherical bubble collapse in viscoelastic fluids," *J. Nonnewton. Fluid Mech.*, vol. 165, no. 1–2, pp. 56–64, 2010.
[7] C. Hua and E. Johnsen, "Nonlinear oscillations following the Rayleigh collapse of a gas bubble in a linear viscoelastic (tissue-like) medium," *Phys. Fluids*, vol. 25, no. 8, 2013.
[8] M. T. Warnez and E. Johnsen, "Numerical modeling of bubble dynamics in viscoelastic media with relaxation," *Phys. Fluids*, vol. 27, no. 6, pp. 1–28, 2015.
[9] Lord Rayleigh, "VIII. On the pressure developed in a liquid during the collapse of a spherical cavity," *London, Edinburgh, Dublin Philos. Mag. J. Sci.*, vol. 34, no. 200, pp. 94–98, Aug. 1917.
[10] J. B. Keller and M. Miksis, "Bubble oscillations of large amplitude," *J. Acoust. Soc. Am.*, vol. 68, no. 2, pp. 628–633, 1980.
[11] N. Phan-Thien and R. I. Tanner, "A new constitutive equation derived from network theory," *J. Nonnewton. Fluid Mech.*, vol. 2, no. 4, pp. 353–365, 1977.
[12] N. Phan-Thien, "A Nonlinear Network Viscoelastic Model," *J. Rheol. (N. Y. N. Y).*, vol. 22, no. 3, pp. 259–283, 1978.
[13] J. G. Oldroyd, "On the Formulation of Rheological Equations of State," *Proc. R. Soc. A Math. Phys. Eng. Sci.*, vol. 200, no. 1063, pp. 523–541, 1950.
[14] B. Budich, S. J. Schmidt, and N. A. Adams, "Numerical simulation and analysis of condensation shocks in cavitating flow," *J. Fluid Mech.*, vol. 838, pp. 759–813, 2018.
[15] G. H. Schnerr, I. H. Sezal, and S. J. Schmidt, "Numerical investigation of three-dimensional cloud cavitation with special emphasis on collapse induced shock dynamics," *Phys. Fluids*, vol. 20, no. 4, pp. 1–9, 2008.
[16] M. S. Mihatsch, S. J. Schmidt, and N. A. Adams, "Cavitation erosion prediction based on analysis of flow dynamics and impact load spectra," *Phys. Fluids*, vol. 27, no. 10, 2015.
[17] I. H. Sezal, "Compressible Dynamics of Cavitating 3-D Multi-Phase Flows," 2009.